Collective plasmon excitations in graphene tubules

Xudong Jiang
Department of Physics and National Laboratory of Mesoscopic Physics, Peking University, Beijing 100871, China
(Received 13 May 1996; revised manuscript received 29 July 1996)

Due to the inherent simplicity of the graphene tubule systems, it is expected that these systems will become model systems for the calculation of the mechanical and electronic properties of idealized carbon fibers. In this paper the collective electronic excitations on graphene tubules are discussed. The frequencies of the plasmons on graphene tubules are calculated using an empirical infinitely thin cylindrical-shell model within the framework of a two-fluid hydrodynamic description. There are two parameters involved in our calculation which are calibrated on graphite. The variations of plasmon frequencies and oscillator strength with the size of tube and longitudinal plasmon wavelength are discussed. [S0163-1829(96)08143-X]

The discovery[1] and the large-scale synthesis[2] of carbon nanometer-size tubes have provided a big boost to research in the area of carbon fiber growth as well as in the production and characterization of fullerene-related materials. Each carbon tube comprises coaxial tubes of graphite sheet, ranging in number from 2 up to 50.[1] As shown by Saito *et al.*,[3] the stacking of graphitic sheets in carbon tubes is turbostratic. That is to say, neighboring graphitic sheets are parallel to each other, but translational and rotational correlations within a sheet plane are random. The concept ''graphene tubule'' is used to refer to a single layer of the honeycomb graphite structure that is rolled in the form of a cylinder, as mentioned by Dresselhaus, Dresselhaus, and Saito.[4] Hence each carbon tube consists of a set of graphene tubules. Due to the inherent simplicity of the graphene tubule systems, it is expected that these systems will become model systems for the calculation of the mechanical and electronic properties of idealized carbon fibers of interest to both the science and application of carbon fibers for practical use. The study of collective excitations is very important in understanding the electron interactions in carbon nanotubes. Ever since the discovery of carbon nanotubes, a lot of experimental[5–7] and theoretical[8–11] work has been done to study the collective electronic plasma excitations in these systems.

The hydrodynamical model was first introduced by Bloch[12] as a generalization of the hydrostatic Thomas-Fermi theory. It was initially applied to the energy lost by fast charged particles to heavy atoms. Through the work of Jensen,[13] this model has begun to be used directly in the calculation of normal modes of electron gas (for a review of this model, see Ref. 14). This model is based on a very clear physical intuition and is considerably simpler than other methods. It gives a good description of the collective modes, both surface and bulk, without the complication of single-particle spectra and it describes the observed features in electron-energy-loss spectroscopy rather well. Barton and Eberlein used this model to propose plasma spectroscopy for C_{60} and C_{70}.[15] The existence of the giant plasmon resonance predicted by them was verified by the photoionization spectra.[16] In this paper we use an empirical infinitely thin cylindrical-shell model to discuss the plasma spectroscopy for a graphene tubule within the framework of a two-fluid hydrodynamic description.

In our model, the graphene tubule is viewed as a hollow cylindrical shell having the same number n of carbon atoms per unit area as the hexagonal plane in graphite. Due to the large aspect ratio,[1] the role of caps is ignored. We take the cylindrical coordinates r, z, and θ. The $\pi(\sigma)$ electrons of graphene tubules are modeled as a continuous fluid with charge $ne(3ne)$ and mass $n\mu_e(3n\mu_e)$ per unit area, superimposed on a uniform, immobile, overall-neutralizing positive background, both confined to the surface of a cylinder of radius r_0. Thus we construct a hydrodynamic model featuring a π fluid and a σ fluid. The displacements of the two fluids from equilibrium are $\boldsymbol{\xi}_\pi = -\nabla_\parallel \phi_\pi(t,\theta)$ and $\boldsymbol{\xi}_\sigma = -\nabla_\parallel \phi_\sigma(t,\theta)$, where $\nabla_\parallel$ differentiates only tangentially. All equations are linearized in ϕ. We also introduce phenomenologically two frequencies $\omega_{r\pi}$ and $\omega_{r\sigma}$, which parametrize the harmonic restoring forces for π and σ electrons, respectively, if both fluids are netural (and therefore uncoupled). These two parameters are fitted to graphite.

We first focus on the description of π fluid, the result of which can be generated to σ electrons directly. The net π surface charge density is $-ne\nabla\cdot\boldsymbol{\xi} = ne\nabla_\parallel^2\phi_\pi$. In terms of the electric field $\mathbf{E} = -\nabla_\parallel \psi$, Newton's second law for modes of circular frequency ω yields

$$n\mu_e(\omega^2 - \omega_{r\pi}^2)\nabla_\parallel \phi_\pi = -ne\nabla_\parallel \psi. \tag{1}$$

Integrating Eq. (1), we get

$$\phi_\pi(t,\theta) = -\frac{e}{\mu_e(\omega^2 - \omega_{r\pi}^2)}\psi(t,r_0,\theta). \tag{2}$$

The requisite solutions of the Laplace equation $\nabla^2\psi = 0$ are

$$\psi = \begin{cases} \sum_{m,q} a_{mq} I_m(qr) e^{im\theta} e^{iqz}, & \text{if } r \leqslant r_0 \\ \sum_{m,q} b_{mq} K_m(qr) e^{im\theta} e^{iqz}, & \text{if } r > r_0 \end{cases} \tag{3}$$

where $I_m(qr)$ and $K_m(qr)$ are modified Bessel functions. $\phi_{\pi,\sigma}$ is defined only at $r = r_0$, which is

$$\phi_{\pi,\sigma} = \sum_{m,q} c_{mq(\pi,\sigma)} e^{im\theta} e^{iqz}, \tag{4}$$

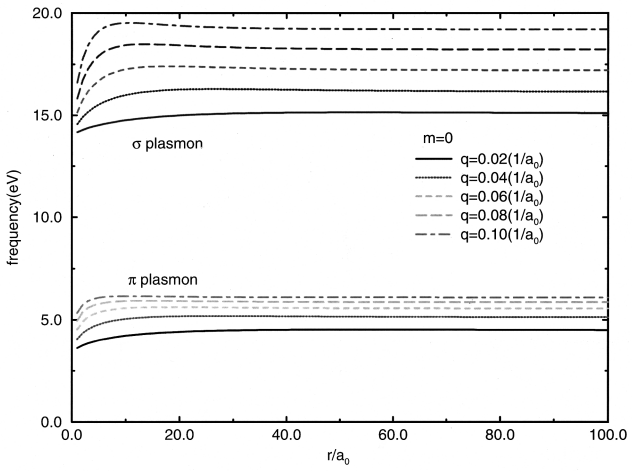

FIG. 1. Variation of $m=0$ plasmon frequencies with tubule radius for several different q's. The upper part corresponds to σ plasmon and the lower part corresponds to π plasmon.

Across the shell ψ is continuous, which means

$$a_{mq}I_m(qr_0)=b_{mq}K_m(qr_0). \tag{5}$$

From Eqs. (2)–(4), one gets

$$c_{mq\pi}=-\frac{e}{\mu_e(\omega^2-\omega_{r\pi}^2)}a_{mq}I_m(qr_0). \tag{6}$$

Similarily, we get

$$c_{mq\sigma}=-\frac{e}{\mu_e(\omega^2-\omega_{r\sigma}^2)}a_{mq}I_m(qr_0). \tag{7}$$

Gauss's law reads

$$\varepsilon_2E_r(r_0+0)-\varepsilon_1E_r(r_0-0)=4\pi ne(\nabla_\parallel^2\phi_\pi+3\nabla_\parallel^2\phi_\sigma), \tag{8}$$

where ε_2 and ε_1 are the dielectric constants outside and inside the graphene tubue, respectively.

Substituting Eqs. (5), (6), and (7) into (8), it finally yields

$$1=\omega_{mq}^2\left[\frac{1}{\omega^2-\omega_{r\pi}^2}+\frac{3}{\omega^2-\omega_{r\sigma}^2}\right], \tag{9}$$

where

$$\omega_{mq}^2=\frac{\dfrac{4\pi ne^2}{\mu_e r_0}(m^2+q^2r_0^2)I_m(qr_0)K_m(qr_0)}{-\varepsilon_2 I_m(qr_0)\dfrac{dK_m}{dr}\bigg|_{r_0}+\varepsilon_1 K_m(qr_0)\dfrac{dI_m}{dr}\bigg|_{r_0}}. \tag{10}$$

In the case of $\varepsilon_2=\varepsilon_1=1$, Eq. (10) becomes[8,10]

$$\omega_{mq}^2=\frac{4\pi ne^2}{\mu_e r_0}(m^2+q^2r_0^2)I_m(qr_0)K_m(qr_0) \tag{11}$$

and we will consider this situation.

Before further investigation, let us turn to consider the plasma spectra of graphite. Crystalline graphite has two plasma frequencies for electric fields parallel to the hexagonal planes,[17–20] with $\hbar\omega_\pi=7$ eV and $\hbar\omega_\sigma=28$ eV; they are

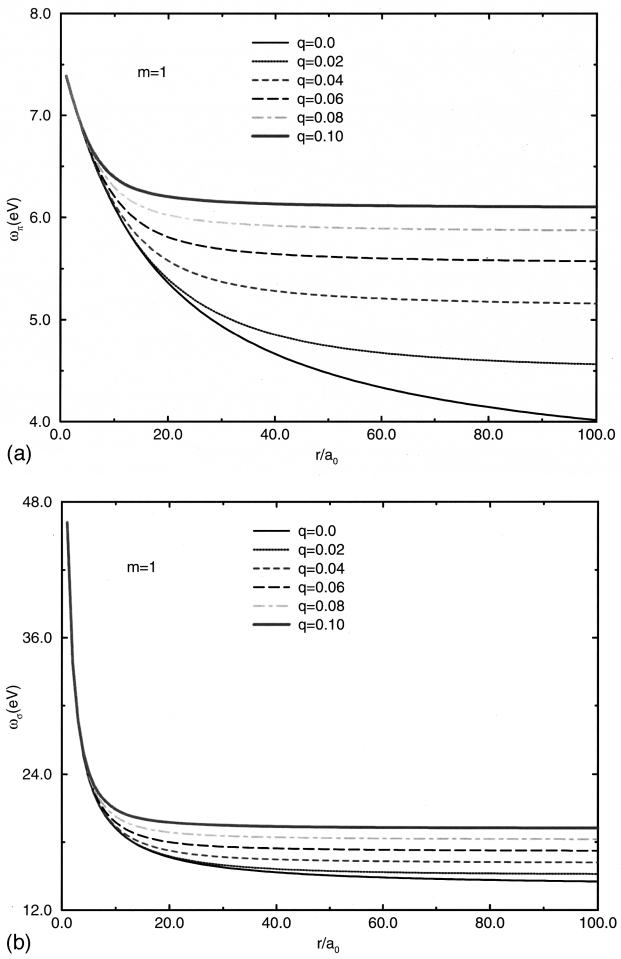

FIG. 2. Variation of $m=1$ plasmon frequencies with the radii of graphene tubules. (a) π plasmon; (b) σ plasmon.

ascribed primarily to the π and σ electrons, numbering υ and 3υ per unit volume, respectively. The free-electron theory predicts plasma peaks at $\sim$12 eV and $\sim$21 eV for the π and σ bands, respectively. The screening effects of the σ electrons in graphite force the two plasma peaks apart, to occur at the experimentally observed values of 7 eV and 28 eV. To allow for screening, a hydrodynamic model featuring a π fluid and a σ fluid was introduced.[15] Similiar to deducing the eigenmode frequency equation for a graphene tubule, the one for graphite is obtained,

$$1=\omega_p^2\left[\frac{1}{\omega^2-\omega_{r\pi}^2}+\frac{3}{\omega^2-\omega_{r\sigma}^2}\right], \tag{12}$$

i.e.,

$$\omega^4-(4\omega_p^2+\omega_{r\pi}^2+\omega_{r\sigma}^2)\omega^2+\omega_{r\pi}^2\omega_{r\sigma}^2+(3\omega_{r\pi}^2+\omega_{r\sigma}^2)\omega_p^2=0, \tag{13}$$

where $\omega_p\equiv\sqrt{4\pi\upsilon e^2/\mu_e}$ is the free-electron plasmon frequency for π electrons.

Fitting the lower root of Eq. (13) to ω_π and the higher one to ω_σ, we find $\hbar\omega_{r\pi}=3.4$ eV and $\hbar\omega_{r\sigma}=14$ eV. The fact that $\omega_{r\pi}$ is much less than $\omega_{r\sigma}$ indicates less localization of π electrons.

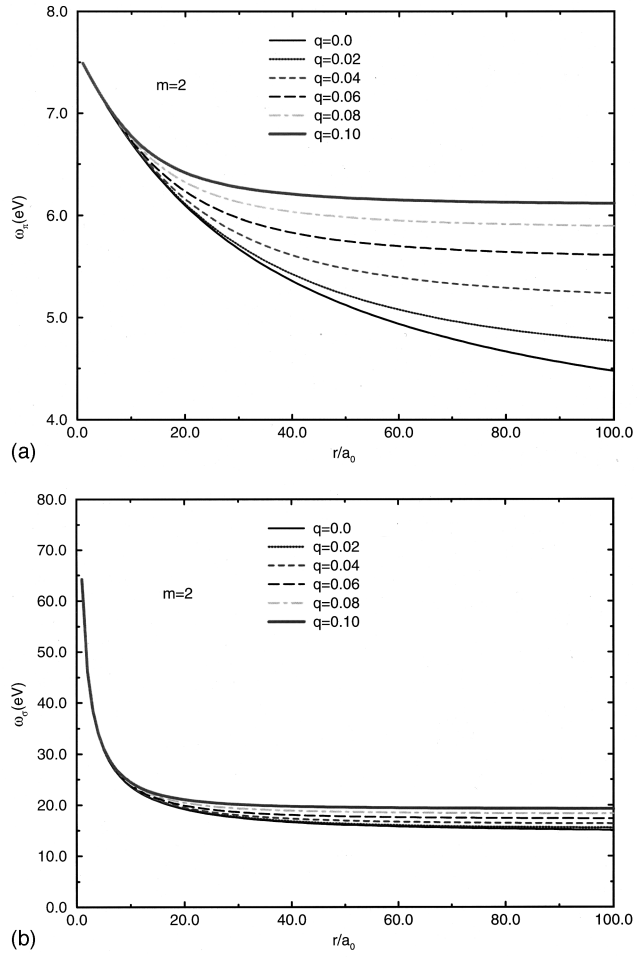

FIG. 3. Variation of $m=2$ plasmon frequencies with the radii of graphene tubules. (a) π plasmon; (b) σ plasmon.

Having gotten $\omega_{r\pi}$ and $\omega_{r\sigma}$, it is easy to solve Eq. (9), which we rewrite in the form

$$\omega^4-(\omega_{r\pi}^2+\omega_{r\sigma}^2+4\omega_{mq}^2)\omega^2+\omega_{r\pi}^2\omega_{r\sigma}^2 + \omega_{mq}^2(\omega_{r\sigma}^2+3\omega_{r\pi}^2)=0. \quad (14)$$

The frequencies of the (m,q) π and σ plasmon are denoted as $\Omega_{mq\pi}$ and $\Omega_{mq\sigma}$, respectively.

Figure 1 shows the variation of $m=0$ plasmon frequencies with the radii of the tubules for different q's. When $qr_0 \ll 1$, $\omega_{mq} \sim q$ and the plasmon excitations have traditional one-dimensional (1D) characters.[8] When $qr_0 \gg 1$, $\omega_{mq} \sim \sqrt{q}$ and the plasmon excitations exhibit 2D behaviors. In such a case the plasmon frequencies are independent of the dimensions of the tubules as can be seen from this figure. Figures 2 and 3 display the variation of plasmon frequencies with the radii of tubules for several q's with $m=1$ and 2, respectively. From the two figures it is found that when $qr_0 \ll 1$, the plasmon (both π and σ) frequencies depend strongly on the radii of the tubules and weakly on q and this is the 1D case.[8] When $qr_0 \gg 1$, the plasmon frequencies depend weakly on the radii of tubules and this corresponds to a 2D case. One can see from Figs. 1–3 a dimensionality crossover as the radii of tubules increase. Also it is found from Figs. 1–3 that

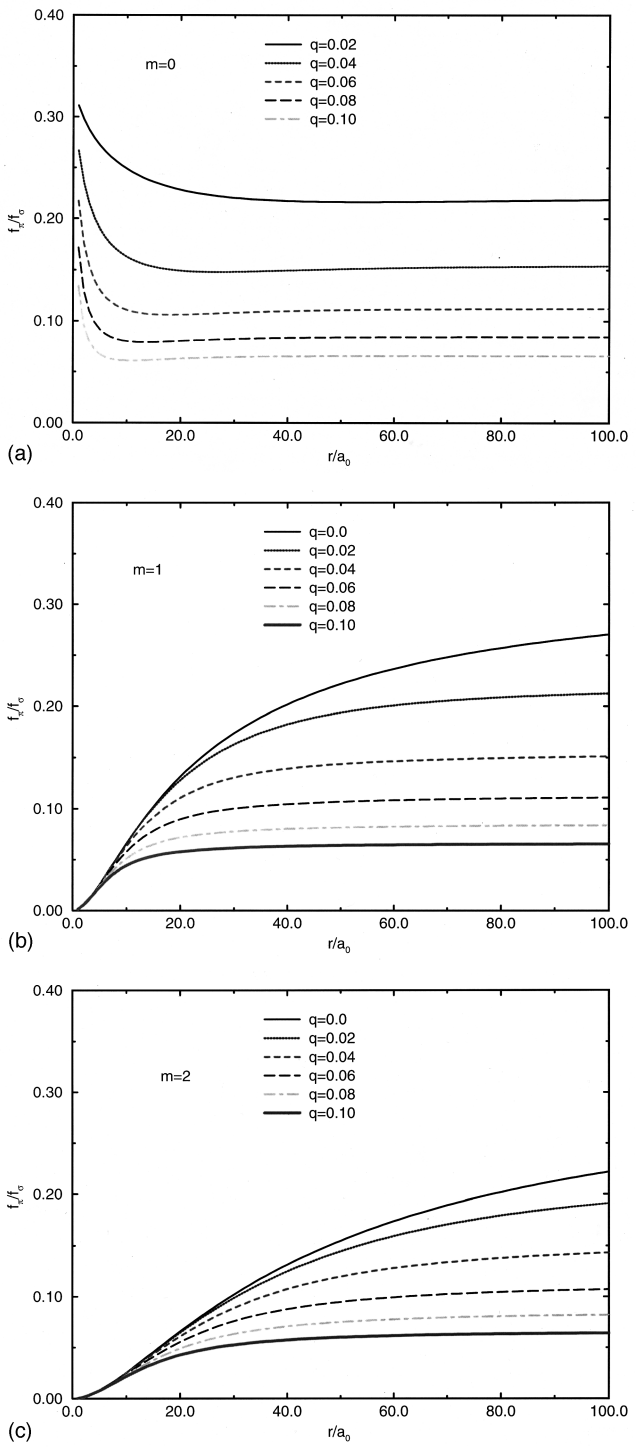

FIG. 4. Variation of the ratio of oscillator strengths between π and σ plasmon with the radii of graphene tubules. (a) $m=0$; (b) $m=1$; (c) $m=2$.

the plasmon frequencies for different m's increase with q, which indicates the important role of longitudinal momentum transfer.

Now, let us consider the polarizability of the graphene tubule. From Eq. (2), we know that at $\omega=\omega_{r\pi}$ there can be no tangential field and this is also true for $\omega=\omega_{r\sigma}$. The polarizability at these frequencies in a homogeneous field is the same as the static polarizability for a perfectly conduct-

ing cylinder in a homogeneous field, namely $r_0^2/2$ per unit length in the z direction. Hence the dynamic polarizability is

$$\alpha_{mq}(\omega)=\frac{r_0^2}{2}\left[g_{mq\pi}\frac{\Omega_{mq\pi}^2}{\Omega_{mq\pi}^2-\omega^2}+g_{mq\sigma}\frac{\Omega_{mq\sigma}^2}{\Omega_{mq\sigma}^2-\omega^2}\right], \tag{15}$$

where

$$g_{mq\pi}=\frac{(\Omega_{mq\pi}^2-\omega_{r\pi}^2)(\omega_{r\sigma}^2-\Omega_{mq\pi}^2)}{\Omega_{mq\pi}^2(\Omega_{mq\sigma}^2-\Omega_{mq\pi}^2)},$$

$$g_{mq\sigma}=\frac{(\Omega_{mq\sigma}^2-\omega_{r\pi}^2)(\Omega_{mq\sigma}^2-\omega_{r\sigma}^2)}{\Omega_{mq\sigma}^2(\Omega_{mq\sigma}^2-\Omega_{mq\pi}^2)}. \tag{16}$$

The combined oscillator strength $f_{mq}=-(\mu_e/e^2)\lim_{\omega\to\infty}\omega^2\alpha_{mq}$ is

$$f_{mq}=\frac{r_0^2}{2}\frac{\mu_e}{e^2}[g_{mq\pi}\Omega_{mq\pi}^2+g_{mq\sigma}\Omega_{mq\sigma}^2]. \tag{17}$$

The ratio of oscillator strengths between π and σ plasma is

$$\gamma_{mq}=\frac{g_{mq\pi}\Omega_{mq\pi}^2}{g_{mq\sigma}\Omega_{mq\sigma}^2}. \tag{18}$$

Figure 4 shows the variation of the ratio of oscillator strengths between π and σ plasmons with the radii of the tubules. From Fig. 4 it is found that the ratios decrease with q for different m's. When $qr_0\gg 1$, the ratios depend weakly on the radius of tubules, corresponding to a 2D character. When $qr_0\ll 1$, the ratios depend strongly on the radii of tubules and in the case of $m=0$ the ratios decrease with r_0, while in the case of $m\neq 0$ the ratios increase with r_0. In fact one can obtain from Eqs. (11), (16), and (18) that when $qr_0\ll 1$, $\gamma_{mq}\sim 1/3[1.0-8\pi ne^2q^2r_0/\mu_e(\omega_{r\sigma}^2-\omega_{r\pi}^2)]$ in the case of $m=0$ and will decrease with r_0, whereas $\gamma_{mq}\sim r_0^2$ in the case of $m\neq 0$ and will increase with r_0. Therefore it is expected that γ_{mq} will exhibit different behaviors in $m=0$ and $m\neq 0$ cases.

[1] S. Iijima, Nature (London) **354**, 56 (1991).
[2] T. W. Ebbesen and P. M. Ajayan, Nature (London) **358**, 220 (1992).
[3] Y. Saito, T. Yoshikawa, S. Bandow, M. Tomita, and T. Hayashi, Phys. Rev. B **48**, 1907 (1993).
[4] M. S. Dresselhaus, G. Dresselhaus, and R. Saito, Phys. Rev. B **45**, 6234 (1992).
[5] L. A. Bursill, P. A. Stadelmann, J. L. Peng, and S. Prawer, Phys. Rev. B **49**, 2882 (1994).
[6] P. M. Ajayan, S. Iijima, and T. Ichihashi, Phys. Rev. B **47**, 6859 (1993).
[7] R. Kuzuo, M. Terauchi, and M. Tanaka, Jpn. J. Appl. Phys. **31**, L1484 (1992).
[8] C. Yannouleas, E. N. Bogachek, and U. Landman, Phys. Rev. B **53**, 10 225 (1996).
[9] C. Yannouleas, E. N. Bogachek, and U. Landman, Phys. Rev. B **50**, 7977 (1994).
[10] P. Longe and S. M. Bose, Phys. Rev. B **48**, 18 239 (1993).
[11] M. F. Lin and W. K. Shung, Phys. Rev. B **47**, 6617 (1993).
[12] F. Bloch, Z. Phys. **81**, 363 (1933).
[13] H. Jensen, Z. Phys. **106**, 620 (1937).
[14] G. Barton, Rep. Prog. Phys. **42**, 963 (1979).
[15] G. Barton and C. Eberlein, J. Chem. Phys. **95**, 1512 (1991).
[16] I. V. Hertel, H. Steger, J. de Vries, B. Weissner, C. Menzel, B. Kamke, and W. Kamke, Phys. Rev. Lett. **68**, 784 (1992).
[17] K. Zeppenfeld, Z. Phys. **243**, 229 (1971).
[18] H. Venghaus, Phys. Status Solidi B **71**, 609 (1935).
[19] Y. H. Ichikawa, Phys. Rev. B **109**, 653 (1958).
[20] E. A. Taft and H. R. Philipp, Phys. Rev. A **138**, 197 (1965).